

# First $^{236}\text{U}$ data from the Arctic Ocean and use of $^{236}\text{U}/^{238}\text{U}$ and $^{129}\text{I}/^{236}\text{U}$ as a new dual tracer

Casacuberta, N.<sup>1\*</sup>, Masqué, P.<sup>2</sup>, Henderson, G.<sup>3</sup>, M. Rutgers van-der-Loeff.<sup>4</sup>, Bauch, D.<sup>5</sup>, Vockenhuber, C.<sup>1</sup>, Daraoui, A.<sup>6</sup>, Walther, C.<sup>6</sup>, Synal, H.-A.<sup>1</sup>, and Christl, M.<sup>1</sup>

<sup>1</sup>Laboratory of Ion Beam Physics, ETH Zurich, Otto Stern Weg 5, 8093 Zurich, Switzerland.

<sup>2</sup>Institut de Ciència i Tecnologia Ambientals & Departament de Física, Universitat Autònoma de Barcelona, 08193 Bellaterra, Spain.

<sup>2</sup>Oceans Institute and School of Physics, The University of Western Australia, 35 Stirling Highway, Crawley, WA 6009, Australia.

<sup>2</sup>School of Natural Sciences & Centre for Marine Ecosystems Research, Edith Cowan University, Joondalup, WA, Australia

<sup>3</sup>Department of Earth Sciences, University of Oxford, South Parks Road, Oxford, OX1 3AN, England.

<sup>4</sup>AWI-Geochemistry, Alfred Wegener Institut Für Polar un Meeresforschung, am Handelshafen 12, 27570, Bremerhaven, Germany.

<sup>5</sup>GEOMAR Helmholtz Centre for Ocean Research Kiel, Wischhofstr. 1-3, 24148 Kiel, Germany.

<sup>6</sup>Institut für Radioökologie und Strahlenschutz, Leibniz Universität Hannover, Herrenhäuser Str. 2 30419 Hannover, Germany.

\* Corresponding author: [ncasacuberta@phys.ethz.ch](mailto:ncasacuberta@phys.ethz.ch)

## ABSTRACT:

The first dataset of  $^{236}\text{U}/^{238}\text{U}$  in the water column of the Arctic Ocean (AO) is presented and shows the widest range of ratios reported so far in the open ocean, from  $(5\pm 5)$  to  $(3840\pm 260) \times 10^{-12}$ . Surface samples and depth profiles were collected during two GEOTRACES expeditions in 2011-2012 and analyzed for the concentrations of  $^{236}\text{U}$  and  $^{129}\text{I}$ , with the aim of investigating whether the combination of  $^{236}\text{U}/^{238}\text{U}$  and  $^{129}\text{I}/^{236}\text{U}$  can be used as a new oceanographic tool in the AO. Results show that the distributions of the  $^{236}\text{U}/^{238}\text{U}$  and  $^{129}\text{I}/^{236}\text{U}$  atomic ratios are consistent with the different water masses in the AO. High  $^{236}\text{U}/^{238}\text{U}$  and  $^{129}\text{I}/^{236}\text{U}$  ratios in the upper water column ( $>2000 \times 10^{-12}$  and  $>200$ , respectively) illustrate the penetration of Atlantic waters (AW) into the AO. Lower values were found in Pacific waters (PW) and deep waters of the AO. Rivers seem to represent a temporally and spatially-constrained third anthropogenic source of  $^{236}\text{U}$  but more data is needed to confirm this. In a simple

mixing model, the combination of  $^{236}\text{U}/^{238}\text{U}$  and  $^{129}\text{I}/^{236}\text{U}$  reveals a high contribution (>99%) of natural background waters (pre-nuclear era) in the deep and bottom waters of the Amerasian basin, indicating an apparent water mass renewal time of > 1000 years. Despite the relatively high apparent age of the Amerasian Basin deep waters, this work shows the potential of using the dual-tracer approach as a new oceanographic tool in the Arctic Ocean.

**Keywords:**  $^{236}\text{U}$ ,  $^{129}\text{I}$ , Arctic Ocean, tracers, GEOTRACES

## 1. INTRODUCTION:

In recent years, an increasing number of studies have measured the anthropogenic occurrence of  $^{236}\text{U}$  ( $T_{1/2}=23$  Ma) in the ocean and indicated its potential as an oceanographic tracer<sup>1-4</sup>. The general suitability of  $^{236}\text{U}$  on a basin-wide scale has been demonstrated recently with the presentation of a first transect through the western North Atlantic Ocean<sup>5</sup>. The strengths of  $^{236}\text{U}$  as an oceanographic tracer are: i) U is soluble (hence conservative) in seawater due to its occurrence as a stable carbonate ion complex,  $\text{UO}_2(\text{CO}_3)_3^{4-}$  and there are currently no indications that  $^{236}\text{U}$  and natural U behave differently in the ocean<sup>3, 6, 7</sup>; ii) contrary to the naturally-occurring U-isotopes, anthropogenic  $^{236}\text{U}$  has not yet reached steady state in the oceans, thus providing a highly dynamic and transient signal penetrating the deep ocean<sup>1</sup>; and iii) due to the incorporation and accumulation of U in aragonite, past  $^{236}\text{U}$  levels can be determined at high-resolution in geological archives such as corals<sup>8</sup>.

On a global scale, the largest source of  $^{236}\text{U}$  is considered to be atmospheric nuclear weapons tests, conducted in the 1950s and 1960s, that released around 1000 kg<sup>9</sup>. Smaller but still significant amounts of  $^{236}\text{U}$  ( $95 \pm 32$  kg) have also been discharged locally into the North Atlantic region by the European nuclear reprocessing facilities of Sellafield, UK and La Hague, France<sup>10</sup>. Other potential sources of  $^{236}\text{U}$  such as discharges from the Russian or former Soviet Union nuclear facilities to Siberian rivers, or contributions from nuclear accidents such as Chernobyl<sup>11</sup> or Fukushima<sup>12</sup>, are thought to be of minor relevance or are not yet documented. Although input functions are currently not well constrained, major efforts have recently been devoted to constrain the  $^{236}\text{U}$  input function from European reprocessing plants, in order to use this radionuclide to track Atlantic waters into the Arctic ocean<sup>10</sup>.

In contrast to  $^{236}\text{U}$ , the major oceanic source of  $^{129}\text{I}$  is not fallout but the liquid discharges from Sellafield and La Hague ( $>6000$  kg since 1970s)<sup>13</sup>, and only about 50 kg of  $^{129}\text{I}$  were released into the atmosphere (and subsequently deposited) as a result of the nuclear weapon tests<sup>14</sup>. Thus, the combination of  $^{236}\text{U}$  with the well-known  $^{129}\text{I}$  pointed to the use of  $^{129}\text{I}/^{236}\text{U}$  as an additional tool in oceanography to constrain water mass sources and transit times. The strengths of combining these two anthropogenic radionuclides are: i) they are both considered to behave conservatively in the open ocean, so variation in their ratios should be water mass dependent<sup>3, 15</sup> and, ii) their different sources and input functions result in very variable  $^{129}\text{I}/^{236}\text{U}$  atomic ratios in time and between sources. Small  $^{129}\text{I}/^{236}\text{U}$  atomic ratio ( $<1$  atom·atom<sup>-1</sup>) can be estimated for global fallout and ratios between 250 and 450 would be representative of the European reprocessing plant releases in the 15 years prior to this study (i.e. from 1998 to 2012)<sup>10</sup>. Apart from their anthropogenic sources, small amounts of natural  $^{236}\text{U}$  and  $^{129}\text{I}$  are present on Earth but their inventories are minor compared to the anthropogenic releases and can be considered to be in steady state with respect to exchange between the different compartments of the global environment. The fractions of naturally occurring  $^{129}\text{I}$  and  $^{236}\text{U}$  in ocean water are referred to as “natural background” in this study, with a corresponding natural  $^{129}\text{I}/^{236}\text{U}$  ratio that would range between 150 and  $\geq 450$ <sup>4, 14</sup>, but mainly characterized by very low  $^{236}\text{U}$  and  $^{129}\text{I}$  concentrations (further details in the discussion).

In this study, the first measurements of  $^{236}\text{U}$  together with  $^{129}\text{I}$  concentrations were made in seawater samples taken in the Arctic Ocean during two GEOTRACES expeditions (ARK XXVI/3 and ARK XXVII/3). The aim is to determine the  $^{129}\text{I}/^{236}\text{U}$  and  $^{236}\text{U}/^{238}\text{U}$  atomic ratios of samples representing different water masses in the Arctic Ocean, and to discuss the implications of using the combination of these ratios as a new tool in oceanography.

## 2. MATERIALS AND METHODS:

**2.1 Samples:** Eight depth profiles and 15 surface seawater samples (Figure 1, Table 1S) were collected in 2011 and 2012 during two *RV Polarstern* expeditions into the Arctic Ocean (ARK XXVI/3 and ARK XXVII/3). Water samples were obtained with 12-L Niskin bottles mounted on a rosette equipped with standard conductivity, temperature

and pressure (CTD) sensors<sup>16, 17</sup>. Between 1 and 10 L samples were collected for <sup>236</sup>U and <sup>129</sup>I-isotope analyses. The unfiltered samples were stored in pre-cleaned (and rinsed with seawater) Nalgene plastic bottles or cubitainers for further processing and analysis.

In August 2014, 4 samples of 1 L each were taken at the mouth of the Lena River, near Tiksi, and upstream of the Stolb Island (Figure 1c). The salinity of these samples was not determined but was probably very low because samples were collected upstream of the normal tidal range of the river.

Surface waters were also analyzed for  $\delta^{18}\text{O}$ . The combination of salinity with oxygen isotopes allows for the determination of the fractions of meteoric water, sea-ice meltwater or brine influence in addition to marine water<sup>18</sup>. In this work, the  $\delta^{18}\text{O}$  data have been used to identify the river fraction in surface waters, indicated in Table 1S.

**2.2 Chemical separation of Uranium and AMS measurement:** Between 1 and 10 L were used for the measurement of <sup>236</sup>U (see Table 1S for details). Samples were weighed, acidified with HNO<sub>3</sub> and spiked with about 3 pg <sup>233</sup>U (IRMM-051). Uranium was pre-concentrated using iron hydroxide co-precipitation. Purification was conducted using pre-packed UTEVA cartridges (Triskem) attached to a vacuum box system to ensure constant operation conditions (e.g. flux of eluate). The purified solutions of U-isotopes were co-precipitated again with about 1-2 mg of iron hydroxide, and transformed to an oxide by heating to 650°C. Finally, samples were mixed with 2-3 mg Nb powder and pressed into the AMS sample holders for U analyses with the compact ETH-Zurich 0.5 MV AMS system Tandy<sup>19</sup>. A total of 6 blanks, each consisting of 100 mL of milliQ water were prepared and treated in the same way as the seawater samples.

The measured U isotopic ratios were normalized to the ETH Zurich in-house standard ZUTRI, with a nominal <sup>236</sup>U/<sup>238</sup>U value of  $(4055 \pm 200) \times 10^{-12}$ <sup>19</sup>. The instrumental background for <sup>236</sup>U/<sup>238</sup>U analyses was estimated to be at the level of  $10^{-14}$ . The measured <sup>236</sup>U/<sup>233</sup>U ratio of the blanks was at a level of  $10^{-5}$  (corresponding to <0.1 fg <sup>236</sup>U). The addition of a <sup>233</sup>U spike allowed for the determination of <sup>236</sup>U and <sup>238</sup>U concentrations.

Five replicate 10 L samples were also analyzed. Results are in good agreement and document the full reproducibility of the method (Table 1, and Figure in supplementary information). We also note that the  $^{236}\text{U}$  analyses of the 0.85 L surface water samples could be performed with a precision of 5 to 13% ( $1\sigma$ ). Results reported in Table 1S from replicates are the averaged values in Table 1 with the corresponding weighted errors.

**2.3 Chemical separation of  $^{129}\text{I}$  and AMS measurement:** From each sample, a subsample of 0.15 L (surface samples), 0.2 L (depths <1000 m) or 0.4 L (depths >1000 m) was separated at ETH Zurich for  $^{129}\text{I}$  analysis. The samples from the deep profiles were sent to IRS Hannover for further preparation<sup>20</sup>, while the surface water samples were processed at ETH Zurich (following the same method).

Between 1.5 and 3 mg of Woodward stable iodine ( $^{127}\text{I}$ ) carrier was added to all samples, and the  $^{129}\text{I}/^{127}\text{I}$  ratio of the spiked samples was determined with the ETH Zurich 0.5 MV AMS system Tandy<sup>21, 22</sup>. The measured  $^{129}\text{I}/^{127}\text{I}$  ratios were normalized to the ETH Zurich in-house standard D22 with a nominal ratio  $^{129}\text{I}/^{127}\text{I} = (50.35 \pm 0.16) \times 10^{-12}$ <sup>19</sup>. Several blanks were prepared showing typical  $^{129}\text{I}/^{127}\text{I}$  ratios of  $(0.2 - 0.3) \times 10^{-12}$  (corresponding to <0.5 fg  $^{129}\text{I}$ ) that were subtracted from the measured ratios (and further calculated concentrations of  $^{129}\text{I}$ ) of the samples.

Four replicate 0.5 L samples were analyzed for samples having very low  $^{129}\text{I}$ , when available. In general, results (Table 1) are in good agreement and document the full reproducibility of the method. Results reported in Table 1S from replicates are the averaged values in Table 1 with the corresponding weighted errors.

### 3. RESULTS:

The  $^{236}\text{U}/^{238}\text{U}$  ratios of the samples collected in 2011/12 in the Arctic Ocean cover the widest range of ratios reported so far in the open ocean<sup>2, 3, 5, 23, 24</sup> (between  $(5 \pm 5)$  and  $(3840 \pm 260) \times 10^{-12}$ , Table 1S, Figure 2). Concentrations of  $^{129}\text{I}$  also display a wide range of values (between  $(0.16 \pm 0.08) \times 10^7$  and  $(804 \pm 10) \times 10^7 \text{ at} \cdot \text{kg}^{-1}$ ) and  $^{129}\text{I}/^{236}\text{U}$  ratios span from  $3 \pm 1$  to  $294 \pm 10$ .

In surface waters, the  $^{236}\text{U}/^{238}\text{U}$  ratios vary between  $(1200\pm100) \times 10^{-12}$  and  $(3840\pm260) \times 10^{-12}$ , with the lowest value corresponding to station 235 (Canada Basin), and the highest ratio found at station 245 (Makarov Basin). Excluding station 235, all surface samples fall between  $2000 \times 10^{-12}$  and  $4000 \times 10^{-12}$ , and are therefore higher than the highest  $^{236}\text{U}/^{238}\text{U}$  ratio observed in both the Atlantic Ocean  $((1400\pm50) \times 10^{-12})$  and the Sea of Japan  $((1600\pm200) \times 10^{-12})^{3,5}$  but lower than the range reported for the North Sea in 2009 (up to  $20 \times 10^{-9}$ )<sup>24</sup> (Figure 2). Results of the eight  $^{236}\text{U}/^{238}\text{U}$  profiles show generally high values in the surface samples ( $>1500$  m) decreasing with depths below 2000 m. The inventories of  $^{236}\text{U}$  in the water column estimated for each individual profile, range from  $12\pm1 \times 10^{12}$  to  $47\pm1 \times 10^{12}$  atom·m<sup>-2</sup> (Table 1S). The lowest inventory corresponds to station 235 in the Canada Basin, while the highest value is calculated for stations 295 and 378 in the Eurasian Basin. All stations located in the Eurasian Basin present larger  $^{236}\text{U}$  inventories than those determined in the Western Atlantic Ocean, where the highest inventory of  $^{236}\text{U}$  was  $39\pm2 \times 10^{12}$  atom·m<sup>-2</sup> at 51°N<sup>1,5</sup>.

A similar distribution is observed for  $^{129}\text{I}/^{236}\text{U}$  atomic ratios, where higher values ( $>100$ ) are observed in surface samples and lower values ( $<15$ ) are observed in deep samples of the Eurasian Basin. However, a different pattern between  $^{236}\text{U}/^{238}\text{U}$  and  $^{129}\text{I}/^{236}\text{U}$  is observed in deep samples of the Amerasian Basin. Whereas  $^{236}\text{U}/^{238}\text{U}$  ratios below 2000 m in stations 226 and 235 are lower than  $50 \times 10^{-12}$ ,  $^{129}\text{I}/^{236}\text{U}$  ratios slightly increase again to up to  $93\pm64$ . Note that the  $^{129}\text{I}/^{236}\text{U}$  ratio taken from the sample at 3500 m depth at station 226 is reported as a low limit, which is calculated from the 1 sigma error of the lowest  $^{129}\text{I}$  and the highest  $^{236}\text{U}$  concentrations.

## 4. DISCUSSION:

### 4.1 General distribution of $^{236}\text{U}/^{238}\text{U}$ and $^{129}\text{I}/^{236}\text{U}$ in the Arctic Ocean in 2011/2012:

Seawater samples taken during 2011 and 2012 in the Arctic Ocean were expected to contain  $^{236}\text{U}$  from global fallout and liquid discharges from European reprocessing plants. Inventories calculated for each single station confirm that the contribution of the latter is prominent in the Arctic Ocean, as inventory values are 2 to 8 times higher than that estimated for fallout contribution for the latitudinal band of 60-90°N of  $5.8 \times 10^{12}$  atom·m<sup>-2</sup><sup>5</sup>. Therefore, atomic ratios of  $^{236}\text{U}/^{238}\text{U}$  and  $^{129}\text{I}/^{236}\text{U}$  distribution in the Arctic Ocean might be explained by different water masses carrying the signal of global

fallout, reprocessing plants, or a mixture between the two sources. This should translate to lower values of  $^{236}\text{U}/^{238}\text{U}$  and  $^{129}\text{I}/^{236}\text{U}$  ( $<2000 \times 10^{-12}$  and  $<0.1$ , respectively) for waters with global fallout input, and higher  $^{236}\text{U}/^{238}\text{U}$  and  $^{129}\text{I}/^{236}\text{U}$  ( $>2000 \times 10^{-12}$ , and  $>200$ , respectively) for waters having a stronger influence from reprocessing plant releases.

The T-S (temperature - salinity) data allows the assignment of water masses to the  $^{236}\text{U}/^{238}\text{U}$  and  $^{129}\text{I}/^{236}\text{U}$  ratios following the water mass definition of Rudels<sup>25</sup> (Figure 3). The color code of each symbol represents the respective  $^{236}\text{U}/^{238}\text{U} \times 10^{-12}$  (Figure 3a) and  $^{129}\text{I}/^{236}\text{U}$  ratios (Figure 3b) of the sample, with cold colors (i.e. purple, blue) for low ratios ( $<600 \times 10^{-12}$ , for  $^{236}\text{U}/^{238}\text{U}$  and  $<60$  for  $^{129}\text{I}/^{236}\text{U}$ ), and warm colors (i.e. red and oranges) for high  $^{236}\text{U}/^{238}\text{U}$  ratios ( $>2600 \times 10^{-12}$ ) and high  $^{129}\text{I}/^{236}\text{U}$  ratios ( $>200$ ). The prominent radionuclide signal from nuclear reprocessing plants is present at depths from the surface to the core of Atlantic Waters ( $<1000$ - $1500$  m) in the Nansen Basin and northern Laptev Sea (stations: 201-212, 224, 250-295 and 378) with high  $^{236}\text{U}/^{238}\text{U}$  ( $>2000 \times 10^{-12}$ ) and  $^{129}\text{I}/^{236}\text{U}$  ( $>200$ ) ratios, especially in the surface. High surface  $^{236}\text{U}/^{238}\text{U}$  and  $^{129}\text{I}/^{236}\text{U}$  ratios observed north of the Laptev Sea are then transported to the Makarov basin (stations 245 and 248) and Amundsen basin (stations 250-259, 218 and 212), reflecting the Transpolar Drift branch of the pan-Arctic boundary current (AOBC). In the Amerasian Basin, Pacific Waters (PW) are represented by low  $^{236}\text{U}/^{238}\text{U}$  ( $(1200 \pm 100) \times 10^{-12}$ ) and low  $^{129}\text{I}/^{236}\text{U}$  ( $13 \pm 1$ ) at the surface of station 235. PW carries less  $^{129}\text{I}$  and  $^{236}\text{U}$ <sup>3, 26</sup> than AW, as the waters from the Pacific Ocean do not carry any  $^{129}\text{I}$  and  $^{236}\text{U}$  from nuclear reprocessing plants, but only from global fallout only<sup>3, 14</sup>.

Note that both  $^{236}\text{U}/^{238}\text{U}$  and  $^{129}\text{I}/^{236}\text{U}$  ratios found in the Arctic Ocean embody a snapshot of the years 2011 and 2012. Specific values for  $^{236}\text{U}/^{238}\text{U}$  and  $^{129}\text{I}/^{236}\text{U}$  cannot be assigned to Arctic water masses due to the time-dependency tracer input function, water circulation and mixing<sup>10</sup>. Yet, the large range of values found in 2011/2012 allows for the discrimination between global fallout and reprocessing plant derived signals (i.e. from  $<0.1$  to  $400$ ). This is one of the features that make the  $^{129}\text{I}/^{236}\text{U}$  atomic ratio an interesting tool to constrain “modern” sources of water masses in the Arctic Ocean.

#### 4.2 Special features observed in the Arctic Ocean using $^{236}\text{U}/^{238}\text{U}$ and $^{129}\text{I}/^{236}\text{U}$ : To

study the contribution of the two principal sources of  $^{236}\text{U}$  and  $^{129}\text{I}$  in the Arctic Ocean in 2011/2012, simple binary endmembers are assumed to delimit a range in  $^{129}\text{I}/^{236}\text{U}$  to  $^{236}\text{U}/^{238}\text{U}$  space in which the water masses are expected to vary (Figure 4). In addition to global fallout (GF) and European reprocessing plants (RP), the natural background (NB) has also been included in the model as described above.

To calculate the  $^{129}\text{I}/^{236}\text{U}$  and  $^{236}\text{U}/^{238}\text{U}$  atomic ratios from the mixing of the different endmembers, the concentrations of  $^{236}\text{U}$ ,  $^{238}\text{U}$  and  $^{129}\text{I}$  are defined for each endmember. These are obtained either from the literature or from our own best estimates (see Table 2). Concentration of U in ocean waters is considered to be constant (3.3 ppb)<sup>27</sup>. We are aware of the fact that the actual U-concentrations, particularly in surface waters of the Arctic Ocean, can be variable (10%)<sup>28</sup> but this additional uncertainty can be neglected given the large uncertainties on the endmember values. The  $^{236}\text{U}/^{238}\text{U}$  and  $^{129}\text{I}/^{236}\text{U}$  ratios of the endmembers are considered to be constant with time for simplicity. Yet, the estimated uncertainty (shaded oval area) of each endmember represents the spatio-temporal variability of both GF and RP. For the GF endmember, the variability accounts for the uneven latitudinal and temporal distribution of radionuclides that were released to the atmosphere by atmospheric bomb tests. The minimum value corresponds to the lowest  $^{236}\text{U}/^{238}\text{U}$  atomic ratio reported for a coral record from Belize at 17°N after 1960<sup>8</sup> and the maximum value corresponds to the highest  $^{236}\text{U}/^{238}\text{U}$  atomic ratio of that coral record (1964), extrapolated to the 30-60°N latitudinal band (where maximum deposition occurred), according to the latitudinal distribution of fallout<sup>29</sup>. This results in the range of  $^{236}\text{U}/^{238}\text{U}$  from global fallout described in Table 2. The uncertainty on the RP endmember is based on the temporal range of discharges of  $^{129}\text{I}$  and  $^{236}\text{U}$  in the last 10 years<sup>10, 30</sup>. Finally, the uncertainty on the NB endmember represents the ranges of calculated values found in the literature<sup>4, 14</sup>. The binary mixing lines between the three endmembers are plotted in a  $^{236}\text{U}/^{238}\text{U}$  vs.  $^{129}\text{I}/^{236}\text{U}$  diagram (Figure 4a).

The measured ratios of all 68 samples are plotted in the  $^{236}\text{U}/^{238}\text{U}$  vs.  $^{129}\text{I}/^{236}\text{U}$  diagram with the binary mixing curves (Figure 4b). Surface samples plot close to the black binary mixing line between GF and RP, confirming that  $^{129}\text{I}$  and  $^{236}\text{U}$  in the surface layers of the Arctic Ocean are dominated by these two sources. The samples lying closer to the RP endmember correspond to surface samples in the Eurasian Basin.



Samples closer to the GF endmember correspond to surface samples from stations 226 and 235 (Amerasian Basin). This observation agrees well with the fact that, due to the longer transit times of waters from the Atlantic Ocean to the Amerasian Basin and due to the presence of PW in the Canada Basin, the local surface waters are more influenced by GF than by RP.

Two special features are observed in this model. The first one concerns some of the surface samples located close to the Laptev Sea (stations 272 - 295) and the Makarov Basin (stations 245 and 248). In particular, surface concentrations of  $^{236}\text{U}$  and  $^{129}\text{I}$  at station 295 are 2-3 times higher than values found in the underlying AW. At all these stations the high radionuclide concentrations correspond to low salinities ( $<32$ ) suggesting a significant freshwater input. Lower salinity surface waters in the Eurasian Basin and Russian coastal seas might be due to the relatively fresh input of the Norwegian Coastal Current (salinities between 31 and 33) and the influence of Russian rivers. Analysis of  $\delta^{18}\text{O}$  and salinity mass balances<sup>18</sup> (and other previous studies using  $\delta^{234}\text{U}$  measurements<sup>31</sup>) confirm that the stations close to the Laptev Sea (280-295) and Makarov Basin (245 and 248) include a considerable fraction of river water (10-12% and 21-22%, respectively, Table 1). These samples are represented in red-edge color in Figure 4b. This could potentially point to a third source of  $^{236}\text{U}$  and  $^{129}\text{I}$ , as already observed for  $^{137}\text{Cs}$  and  $^{129}\text{I}$  in other studies<sup>32</sup>. However, there is currently no way of distinguishing between the Ob, Yenisei and Lena rivers, unless  $^{236}\text{U}$  and  $^{129}\text{I}$  data are available from these rivers. Based on the results from the four samples collected at the mouth of the Lena river (Table 1S), this river was excluded as a source of  $^{236}\text{U}$  and  $^{129}\text{I}$  to the Arctic Ocean in 2011 and 2013. The Ob river, however, is known to be a source of artificial radionuclides to the Arctic Ocean<sup>32, 33</sup>, mainly due to the nuclear wastes of the Mayak nuclear reprocessing plant that have been discharged to the Techa-Iset-Tsobol-Irtysh-Ob River system for many years.  $^{236}\text{U}$  and  $^{129}\text{I}$  concentrations discharged by the Ob River might have changed significantly over time. Nevertheless, maximum  $^{236}\text{U}$  and  $^{129}\text{I}$  concentrations observed at the beginning of the 1990's in the Ob River were  $100 \times 10^6 \text{ at}\cdot\text{L}^{-1}$  ( $\approx 1.2 \times 10^{-5} \text{ }^{236}\text{U}/^{238}\text{U}$ ) and  $2.7 \times 10^9 \text{ at}\cdot\text{kg}^{-1}$ , respectively<sup>33-35</sup>. The Yenisei river could also suffer from radioactive contamination caused by discharges from the Krasnoyarsk Mining and the Chemical Complex at Lake Karachay<sup>36</sup>. The river input (RI) endmember cannot therefore be defined in the diagram, although it should be placed somewhere above the GF-RP binary line due to higher  $^{236}\text{U}/^{238}\text{U}$

atomic ratio. The second feature observed in the binary model concerns the deep and bottom waters of the samples collected in the deep Amerasian Basin. Despite considerable experimental uncertainties due to values close to the detection limit, the deepest samples of stations 226 and 235 in the Canadian and Makarov Basin show increased  $^{129}\text{I}/^{236}\text{U}$  ratios, together with very low  $^{236}\text{U}/^{238}\text{U}$  ratios (Figure 4c). This probably indicates that, despite the uncertainties associated with these measurements, the Amerasian Basin bottom waters consist of a large proportion (about 99%) of waters carrying the  $^{129}\text{I}/^{236}\text{U}$  signal of the NB endmember. The slightly elevated concentration of  $^{129}\text{I}$  found in these samples ( $0.3 - 1 \times 10^7 \text{ at} \cdot \text{kg}^{-1}$ ) can be explained by a contribution of only 1‰ of waters carrying the RP end member signal. The  $^{236}\text{U}$  concentration in these samples would not change significantly by adding such a small contribution of RP waters since the  $^{236}\text{U}/^{238}\text{U}$  levels in the GF and the RP endmembers are similar.

A simple one box model, and assuming that only about 1% of the water volume in the Amerasian Basin has been replaced over the past about 50 years by surface waters, suggests an apparent water mass renewal time more than 1000 years for the deep Amerasian Basin. This value is in rough agreement with earlier findings using pre-bomb surface  $\Delta^{14}\text{C}$  and  $^{39}\text{Ar}$  measurements<sup>37</sup>, which proved the long isolation ages of deep and bottom waters in the Amerasian Basin of 500 years<sup>37-39</sup>. Our data on  $^{129}\text{I}$  and  $^{236}\text{U}$  (and their ratio) is therefore a first approach to prove the potential of using this dual tracer as a sensitive tool to determine vertical mixing processes in the deep Arctic Ocean.

#### **4.3 Strengths and weaknesses of using $^{236}\text{U}/^{238}\text{U}$ and $^{129}\text{I}/^{236}\text{U}$ as an ocean tracer:**

The combination of  $^{236}\text{U}$  and  $^{129}\text{I}$  may provide a new dual tracer tool to: i) constrain sources of water masses; ii) identify additional sources of artificial radionuclides (e.g. river inputs); iii) quantify transit times of AW to the AO and; iv) estimate time scales of vertical mixing processes in the deep AO.

The large range of the  $^{129}\text{I}/^{236}\text{U}$  atomic ratios from the two main endmembers (i.e. GF<0.1 and RP>250) allows for a robust way of identifying the contribution of each source to the AO waters. The identification of other radionuclide sources to the AO should be possible when these show different  $^{236}\text{U}/^{238}\text{U}$  and  $^{129}\text{I}/^{236}\text{U}$  ratio, away from the GF-RP binary line. The potential of calculating transit times of Atlantic waters to

the Arctic Ocean has already been discussed in a separate work<sup>10</sup>, using the dynamics of the transient tracer distribution. This work shows that the combination with  $^{236}\text{U}/^{238}\text{U}$  and  $^{129}\text{I}/^{236}\text{U}$  ratios allows the determination of transit times or tracer ages of Atlantic Waters in the Arctic Ocean over the last two decades<sup>10</sup>. Finally, low concentrations of both  $^{129}\text{I}$  ( $<10^7$  at·kg<sup>-1</sup> and  $^{236}\text{U}$   $<10^6$  at·kg<sup>-1</sup>) combined to high  $^{129}\text{I}/^{236}\text{U}$  ratio ( $>100$ ) indicate old (i.e. pre bomb era) water masses. All this, combined with new developments in Accelerator Mass Spectrometry (AMS)<sup>4, 21, 22</sup> should allow for even more sensitive determinations of  $^{236}\text{U}$  and  $^{129}\text{I}$  in small volume samples<sup>2</sup> with high precision<sup>40</sup>.

The weaknesses of using  $^{236}\text{U}/^{238}\text{U}$  and  $^{129}\text{I}/^{238}\text{U}$  to constrain sources of water masses in the Arctic Ocean by using the simple mixing model are obvious. Most importantly the independent combination of 3 binary mixing lines cannot be used to precisely calculate the relative contribution of each endmember. In addition, the temporal variability of the anthropogenic sources is not considered and the endmembers are currently not very well defined. However, the simple model can still be used to get a general overview of the sources of  $^{236}\text{U}$  and  $^{129}\text{I}$  in the Arctic Ocean and to assess the importance of the different origins. Accordingly, the dominance of the RP source over GF, the minor presence of river input and the weak but non-negligible role of NB, can be considered robust results of the mixing model.

## 5. CONCLUSIONS:

The first dataset of  $^{236}\text{U}$  in Arctic Ocean seawaters is presented, and the use of  $^{236}\text{U}/^{238}\text{U}$  together with  $^{129}\text{I}/^{236}\text{U}$  is shown to provide a new dual tracer of water mass circulation in the Arctic Ocean.  $^{236}\text{U}/^{238}\text{U}$  atomic ratios span the widest range described for open ocean waters (between  $(5\pm5)$  and  $(3840\pm260) \times 10^{-12}$ ) and both  $^{236}\text{U}/^{238}\text{U}$  and  $^{129}\text{I}/^{236}\text{U}$  atomic ratios are consistent with the hydrography and the distribution of the different water masses of the Arctic Ocean.

The combination of  $^{236}\text{U}/^{238}\text{U}$  and  $^{129}\text{I}/^{236}\text{U}$  atomic ratios provides a new approach to distinguish the sources of these two artificial radionuclides that would not be possible with the use of individual  $^{236}\text{U}$  or  $^{129}\text{I}$  concentrations. A simple box model based on the combination of  $^{236}\text{U}/^{238}\text{U}$  and  $^{129}\text{I}/^{236}\text{U}$  ratios allows the identification of Siberian rivers as another source of artificial radionuclides in the Arctic Ocean. Furthermore, this

model shows that the dual tracer approach has the potential of becoming an extremely sensitive tool to study isolation ages of deep and bottom waters of the Amerasian Basin.

But weaknesses of this dual tracer, such as the poor knowledge of the different input functions, need to be overcome. Future sampling campaigns in the AO and elsewhere will help providing more data for  $^{236}\text{U}$  and  $^{129}\text{I}$ , obtaining more information on the time-dependency variable, particularly for the two European reprocessing plants, and constraining the input of these two radionuclides in the Arctic Ocean.

## ACKNOWLEDGEMENTS

The authors acknowledge the chief scientists, colleagues, captain and crew members involved in sampling activities during the two expeditions of the Polarstern, in 2011/2012, and Anton Vaks for the Lena River sampling in 2014. NC research was supported by the ETH Zürich Postdoctoral Fellowship Program and currently by the Swiss National Science Foundation (AMBIZIONE PZ00P2\_154805). PM was supported in part by a Gledten Visiting Fellowship awarded by the Institute of Advanced Studies at The University of Western Australia and by the Generalitat de Catalunya through MERS (2014 SGR 1356). DB acknowledges funding by the German Research Funding Agency DFG (project BA1689). The ETH Zurich Laboratory of Ion Beam Physics is partially funded by its consortium partners EAWAG, EMPA, and PSI.

## REFERENCES:

1. Christl, M.; Lachner, J.; Vockenhuber, C.; Lechtenfeld, O.; Stimac, I.; Rutgers van der Loeff, M.; Synal, H.-A., A depth profile of uranium-236 in the Atlantic Ocean. *Geochim Cosmochim Acta* **2012**, *77*, (0), 98-107.
2. Eigl, R.; Srncik, M.; Steier, P.; Wallner, G.,  $^{236}\text{U}/^{238}\text{U}$  and  $^{240}\text{Pu}/^{239}\text{Pu}$  isotopic ratios in small (2 L) sea and river water samples. *Journal of Environmental Radioactivity* **2013**, *116*, (0), 54-58.
3. Sakaguchi, A.; Kadokura, A.; Steier, P.; Takahashi, Y.; Shizuma, K.; Hoshi, M.; Nakakuki, T.; Yamamoto, M., Uranium-236 as a new oceanic tracer: A first depth profile in the Japan Sea and comparison with caesium-137. *Earth and Planetary Science Letters* **2012**, *333-334*, (0), 165-170.
4. Steier, P.; Bichler, M.; Fifield, K. L.; Golser, R.; Kutschera, W.; Priller, A.; Quinto, F.; Richter, S.; Srncik, M.; Terrasi, P.; Wacker, L.; Wallner, A.; Wallner, G.; Wilcken, K. M.; Wild, E. M., Natural and anthropogenic  $^{236}\text{U}$  in environmental samples. *Nuclear Instruments and Methods in Physics Research Section B: Beam Interactions with Materials and Atoms* **2008**, *266*, (10), 2246-2250.
5. Casacuberta, N.; Christl, M.; Lachner, J.; van der Loeff, M. R.; Masque, P.; Synal, H. A., A first transect of U-236 in the North Atlantic Ocean. *Geochim Cosmochim Acta* **2014**, *133*, 34-46.
6. Rutgers van der Loeff, M. M.; Geibert, W., Chapter 7 U- and Th-Series Nuclides as Tracers of Particle Dynamics, Scavenging and Biogeochemical Cycles in the Oceans. In *Radioactivity in the Environment*, Krishnaswami, S.; Cochran, J. K., Eds. Elsevier: 2008; Vol. Volume 13, pp 227-268.
7. Langmuir, D., Uranium solution-mineral equilibria at low temperatures with applications to sedimentary ore deposits. *Geochim Cosmochim Acta* **1978**, *42*, (6, Part A), 547-569.
8. Winkler, S. R.; Steier, P.; Carilli, J., Bomb fall-out  $^{236}\text{U}$  as a global oceanic tracer using an annually resolved coral core. *Earth and Planetary Science Letters* **2012**, *359-360*, (0), 124-130.
9. Sakaguchi, A.; Kawai, K.; Steier, P.; Quinto, F.; Mino, K.; Tomita, J.; Hoshi, M.; Whitehead, N.; Yamamoto, M., First results on  $^{236}\text{U}$  levels in global fallout. *Science of The Total Environment* **2009**, *407*, (14), 4238-4242.
10. Christl, M.; Casacuberta, N.; Vockenhuber, C.; C., E.; Bailly du Bois, P.; Herrmann, J.; Synal, H. A., Reconstruction of the  $^{236}\text{U}$  input function for the Northeast Atlantic Ocean: Implications for  $^{129}\text{I}/^{236}\text{U}$  and  $^{236}\text{U}/^{238}\text{U}$ -based tracer ages. *Journal of Geophysical Research: Oceans* **2015**.
11. Boulyga, S. F.; Heumann, K. G., Determination of extremely low  $^{236}\text{U}/^{238}\text{U}$  isotope ratios in environmental samples by sector-field inductively coupled plasma mass spectrometry using high-efficiency sample introduction. *Journal of Environmental Radioactivity* **2006**, *88*, (1), 1-10.
12. Sakaguchi, A.; Steier, P.; Takahashi, Y.; Yamamoto, M., Isotopic Compositions of  $^{236}\text{U}$  and Pu Isotopes in "Black Substances" Collected from Roadsides in Fukushima Prefecture: Fallout from the Fukushima Dai-ichi Nuclear Power Plant Accident. *Environmental Science & Technology* **2014**, *48*, (7), 3691-3697.

- 447 13. He, P.; Hou, X.; Aldahan, A.; Possnert, G.; Yi, P., Iodine isotopes species  
448 fingerprinting environmental conditions in surface water along the northeastern  
449 Atlantic Ocean. *Sci. Rep.* **2013**, *3*.
- 450 14. Raisbeck, G. M.; Yiou, F., 129I in the oceans: origins and applications. *Science*  
451 *of The Total Environment* **1999**, 237–238, (0), 31-41.
- 452 15. Aldahan, A.; Alfimov, V.; Possnert, G., 129I anthropogenic budget: Major  
453 sources and sinks. *Applied Geochemistry* **2007**, *22*, (3), 606-618.
- 454 16. Schauer, U. *The Expedition of the Research Vessel "Polarstern" to the Arctic in*  
455 *2011 (ARK-XXVI/3 - TransArc)*; Alfred-Wegener-Institut Für Polar- und  
456 Meeresforschung, 2012, 2012.
- 457 17. Boetius, A. *The Expedition of the Research Vessel "Polarstern" to the Arctic in*  
458 *2012 (ARK-XXVII/3)*; Alfred-Wegener-Institut: Alfred-Wegener-Institut, 2013.
- 459 18. Bauch, D.; van der Loeff, M. R.; Andersen, N.; Torres-Valdes, S.; Bakker, K.;  
460 Abrahamsen, E. P., Origin of freshwater and polynya water in the Arctic Ocean  
461 halocline in summer 2007. *Progress in Oceanography* **2011**, *91*, (4), 482-495.
- 462 19. Christl, M.; Vockenhuber, C.; Kubik, P. W.; Wacker, L.; Lachner, J.; Alfimov, V.;  
463 Synal, H. A., The ETH Zurich AMS facilities: Performance parameters and reference  
464 materials. *Nuclear Instruments and Methods in Physics Research Section B: Beam*  
465 *Interactions with Materials and Atoms* **2013**, *294*, (0), 29-38.
- 466 20. Michel, R.; Daraoui, A.; Gorny, M.; Jakob, D.; Sachse, R.; Tosch, L.; Nies, H.;  
467 Goroncy, I.; Herrmann, J.; Synal, H. A.; Stocker, M.; Alfimov, V., Iodine-129 and  
468 iodine-127 in European seawaters and in precipitation from Northern Germany.  
469 *Science of The Total Environment* **2012**, *419*, (0), 151-169.
- 470 21. Vockenhuber, C.; Alfimov, V.; Christl, M.; Lachner, J.; Schulze-König, T.; Suter,  
471 M.; Synal, H. A., The potential of He stripping in heavy ion AMS. *Nuclear*  
472 *Instruments and Methods in Physics Research Section B: Beam Interactions with*  
473 *Materials and Atoms* **2013**, *294*, (0), 382-386.
- 474 22. Vockenhuber, C.; Casacuberta, N.; Christl, M.; Synal, H.-A., Accelerator Mass  
475 Spectrometry of 129I towards its lower limits. *Nuclear Instruments and Methods in*  
476 *Physics Research Section B: Beam Interactions with Materials and Atoms* **2015**, (0).
- 477 23. Sakaguchi, A. Y. A.; Kadokura, A.; Steier, P.; Tanaka, K.; Takahashi, Y.; Chiga,  
478 H.; Matsushima, A.; Nakashima, S.; Onda, Y., Isotopic determination of U, Pu and Cs  
479 in environmental waters following the Fukushima Daiichi Nuclear Power Plant  
480 accident. *GEOCHEMICAL JOURNAL* **2012**, *46*, (4), 355-360.
- 481 24. Christl, M.; Casacuberta, N.; Lachner, J.; Maxeiner, S.; Vockenhuber, C.; Synal,  
482 H.-A.; Goroncy, I.; Herrmann, J.; Daraoui, A.; Walther, C.; Michel, R., Status of 236U  
483 analyses at ETH Zurich and the distribution of 236U and 129I in the North Sea in  
484 2009. *Nuclear Instruments and Methods in Physics Research Section B: Beam*  
485 *Interactions with Materials and Atoms* **2015**, (0).
- 486 25. Rudels, B., Arctic Ocean Circulation. In *Encyclopedia of Ocean Sciences*  
487 *(Second Edition)*, Steele, J. H., Ed. Academic Press: Oxford, 2009; pp 211-225.
- 488 26. Karcher, M.; Smith, J. N.; Kauker, F.; Gerdes, R.; Smethie, W. M., Recent  
489 changes in Arctic Ocean circulation revealed by iodine-129 observations and  
490 modeling. *Journal of Geophysical Research: Oceans* **2012**, *117*, (C8), C08007.

- 491 27. Pates, J. M.; Muir, G. K. P., U-salinity relationships in the Mediterranean:  
492 Implications for  $^{234}\text{Th}$ : $^{238}\text{U}$  particle flux studies. *Marine Chemistry* **2007**, *106*, (3-  
493 4), 530-545.
- 494 28. Owens, S. A.; Buesseler, K. O.; Sims, K. W. W., Re-evaluating the  $^{238}\text{U}$ -  
495 salinity relationship in seawater: Implications for the  $^{238}\text{U}$ - $^{234}\text{Th}$  disequilibrium  
496 method. *Marine Chemistry* **2011**, *127*, (1-4), 31-39.
- 497 29. UNSCEAR *Sources and Effects of Ionizing Radiation*; 2000.
- 498 30. Christl, M., Casacuberta, N., Vockenhuber, C., Synal, H.-A., Bailly du Bois, P.,  
499 Elsässer, C., Herrmann, J., Reconstruction of the U-236 input into the Northeast  
500 Atlantic Ocean and implications for  $^{129}\text{I}$ / $^{236}\text{U}$  and  $^{236}\text{U}$ / $^{238}\text{U}$  based tracer ages.  
501 *Journal of Geophysical Research: Oceans* **under revision**.
- 502 31. Andersen, M. B.; Stirling, C. H.; Porcelli, D.; Halliday, A. N.; Andersson, P. S.;  
503 Baskaran, M., The tracing of riverine U in Arctic seawater with very precise  
504  $^{234}\text{U}$ / $^{238}\text{U}$  measurements. *Earth and Planetary Science Letters* **2007**, *259*, (1-2),  
505 171-185.
- 506 32. Cooper, L. W.; Beasley, T.; Aagaard, K.; Kelley, J. M.; Larsen, I. L.; Grebmeier,  
507 J. M., Distributions of nuclear fuel-reprocessing tracers in the Arctic Ocean:  
508 Indications of Russian river influence. *Journal of Marine Research* **1999**, *57*, (5),  
509 715-738.
- 510 33. Moran, S. B.; Cochran, J. K.; Fisher, N. S.; Kilius, L. R., I-129 in the Ob River. In  
511 *Environmental Radioactivity in the Arctic*, Norwegian Radiation Protection Agency:  
512 Oslo, 1995.
- 513 34. Cooper, L. W.; Kelley, J. M.; Bond, L. A.; Orlandini, K. A.; Grebmeier, J. M.,  
514 Sources of the transuranic elements plutonium and neptunium in arctic marine  
515 sediments. *Marine Chemistry* **2000**, *69*, (3-4), 253-276.
- 516 35. Beasley, T. M.; Kelley, J. M.; Orlandini, K. A.; Bond, L. A.; Aarkrog, A.;  
517 Trapeznikov, A. P.; Pozolotina, V. N.; Beasley, T. M.; Kelley, J. M.; Orlandini, K. A.;  
518 Bond, L. A.; Aarkrog, A.; Trapeznikov, A. P.; Pozolotina, V. N., Isotopic Pu, U, and Np  
519 signatures in soils from Semipalatinsk-21, Kazakh Republic and the Southern  
520 Urals, Russia. *J. Environ. Radioact.* **1998**, *39*, 215-230.
- 521 36. Aarkrog, A.; Aarkrog, A., Worldwide marine radioactivity studies  
522 (WOMARS). Radionuclide levels in oceans and seas. In *Worldwide marine*  
523 *radioactivity studies (WOMARS). Radionuclide levels in oceans and seas*, 2005; Vol.  
524 IAEA-TECDOC-1429.
- 525 37. Schlosser, P.; Kromer, B.; Ostlund, G.; Ekwurzel, B.; Boenisch, G.; Loosli, H.  
526 H.; Purtschert, R., *On the  $^{14}\text{C}$  and  $^{39}\text{Ar}$  distribution in the central Arctic Ocean;*  
527 *implications for deep water formation*. 2006.
- 528 38. Macdonald, R. W.; Carmack, E. C.; Wallace, D. W. R., Tritium and  
529 Radiocarbon Dating of Canada Basin Deep Waters. *Science* **1993**, *259*, (5091), 103-  
530 104.
- 531 39. Schlosser, P.; Kromer, B.; Ekwurzel, B.; Bönnisch, G.; McNichol, A.; Schneider,  
532 R.; von Reden, K.; Östlund, H. G.; Swift, J. H., The first trans-Arctic  $^{14}\text{C}$  section:  
533 comparison of the mean ages of the deep waters in the Eurasian and Canadian

534 basins of the Arctic Ocean. *Nuclear Instruments and Methods in Physics Research*  
535 *Section B: Beam Interactions with Materials and Atoms* **1997**, 123, (1–4), 431-437.  
536 40. Christl, M.; Vockenhuber, C.; Kubik, P. W.; Wacker, L.; Lachner, J.; Alfimov, V.;  
537 Synal, H. A., The ETH Zurich AMS facilities: Performance parameters and reference  
538 materials. *Nucl. Instrum. Methods Phys. Res., Sect. B* **2013**, 294, 29-38.  
539  
540  
541  
542



Figure 1: a) Map of the Arctic Ocean showing the sampling locations and the general pattern of the surface circulation; black arrows represent Pacific Waters and white arrows are indicative of major rivers discharging into the Arctic Ocean; b) Detailed map of the Arctic Ocean to indicate locations of samples more clearly. Samples taken during *RV Polarstern* expeditions ARK XXVI/3 are indicated in blue and samples from ARK XXVII/3 are indicated in red. Deep profiles are indicated with black circles; c) Location map for the Lena-Delta region showing the sampling sites for the three rivers and one coastal sample analysed in this study.

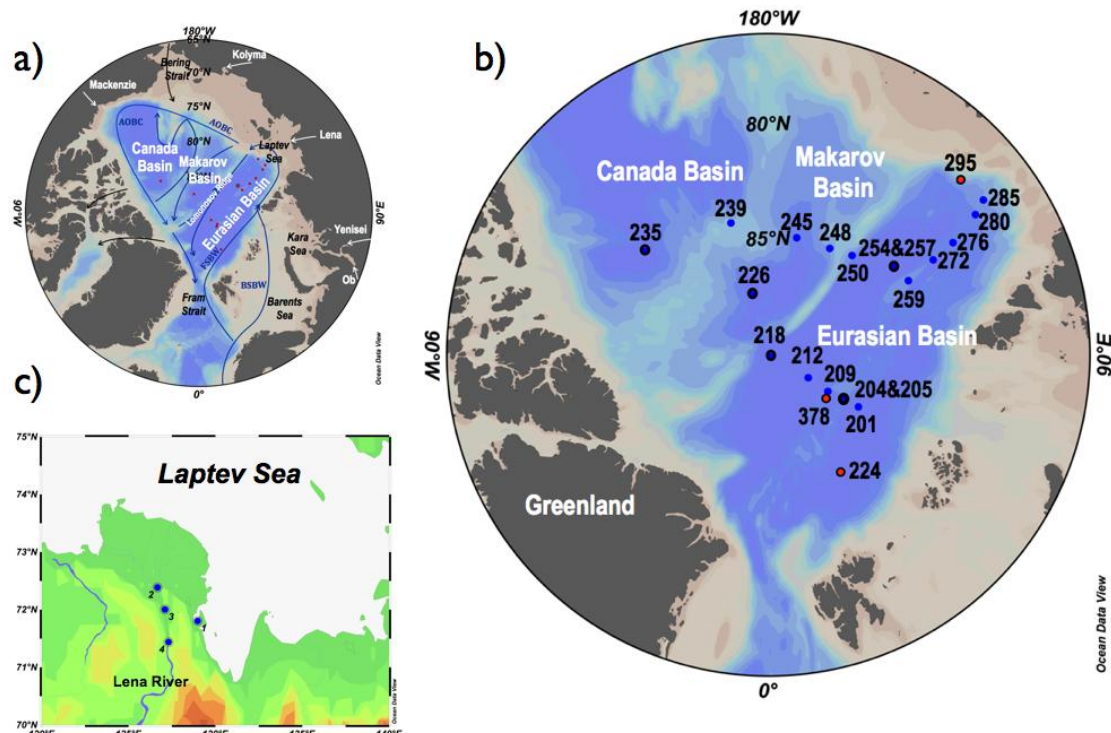


Figure 2: Reported values of  $^{236}\text{U}/^{238}\text{U}$  in seawater samples from different locations (i.e. Atlantic Ocean, Sea of Japan, Pacific Ocean, Black Sea, Irish Sea and North Sea), including this study. Blue bar indicates the average and red bar indicates the median value of all samples in this study. Note that x-axis is in logarithmic scale.

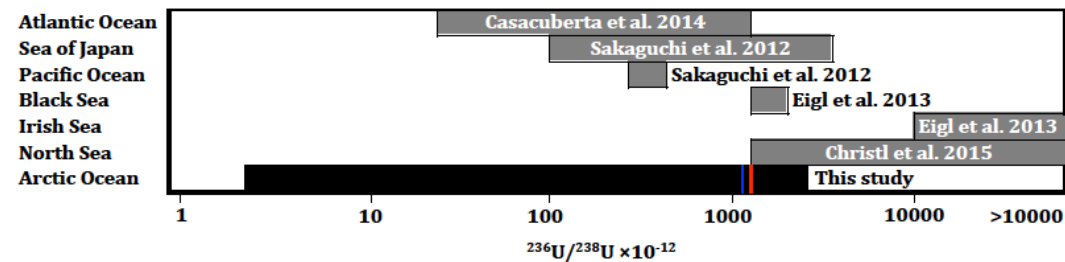


Figure 3: T-S plots of surface samples and 8 depth profiles taken for  $^{236}\text{U}$  and  $^{129}\text{I}$  radionuclide analysis during *RV Polarstern* expeditions the ARK XXVI/3 and ARK XXVII/3. Samples of the 8 profiles are represented with different symbols and T-S data of the depth profiles is shown in grey lines (a). Surface samples are shown as colored dots. The colors of each symbol show a)  $^{236}\text{U}/^{238}\text{U}$  ratio ( $\times 10^{-12}$ ) and b)  $^{129}\text{I}/^{236}\text{U}$  ratio. T-S ranges of water masses are indicated following<sup>25</sup>. The individual T-S data for each station are available at pangea.org.

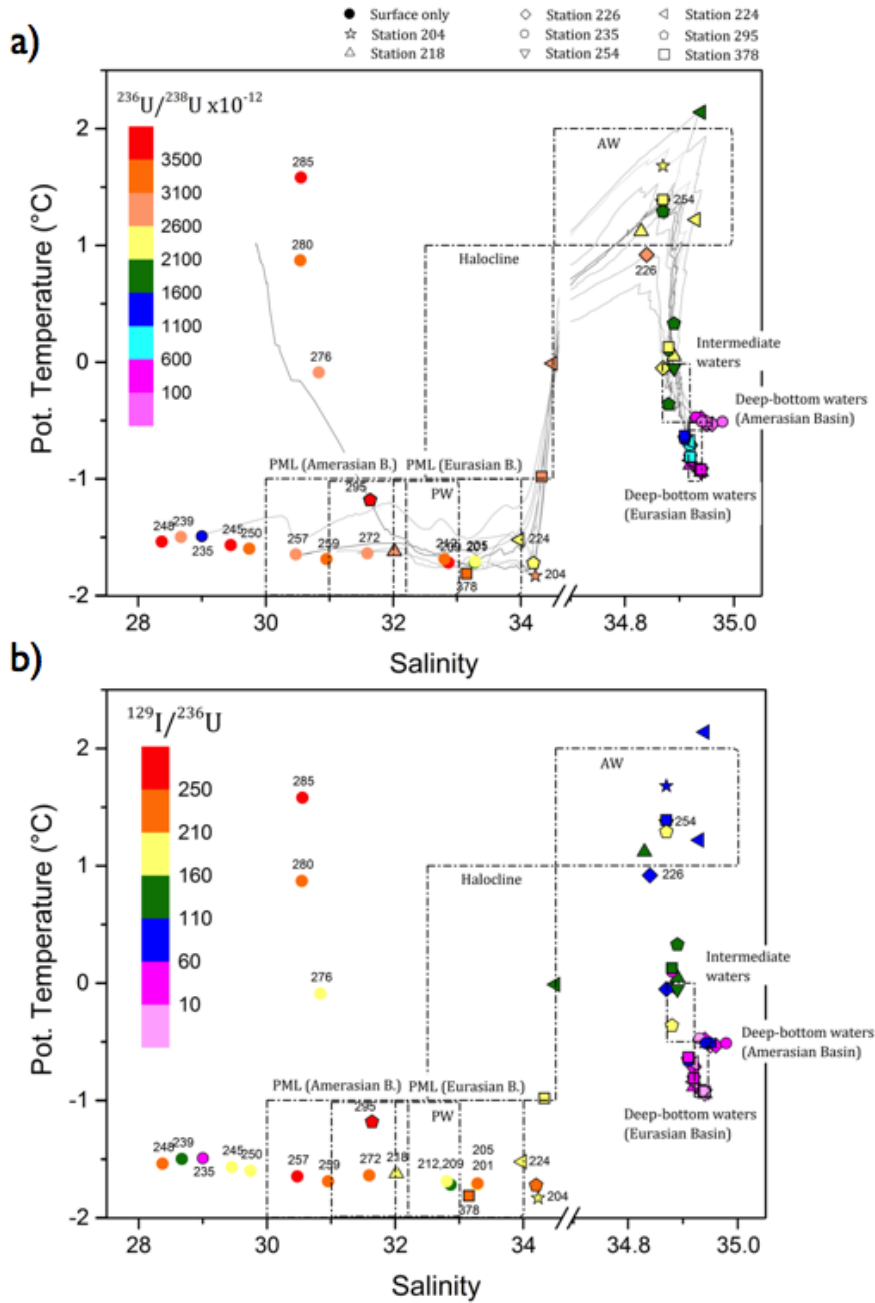
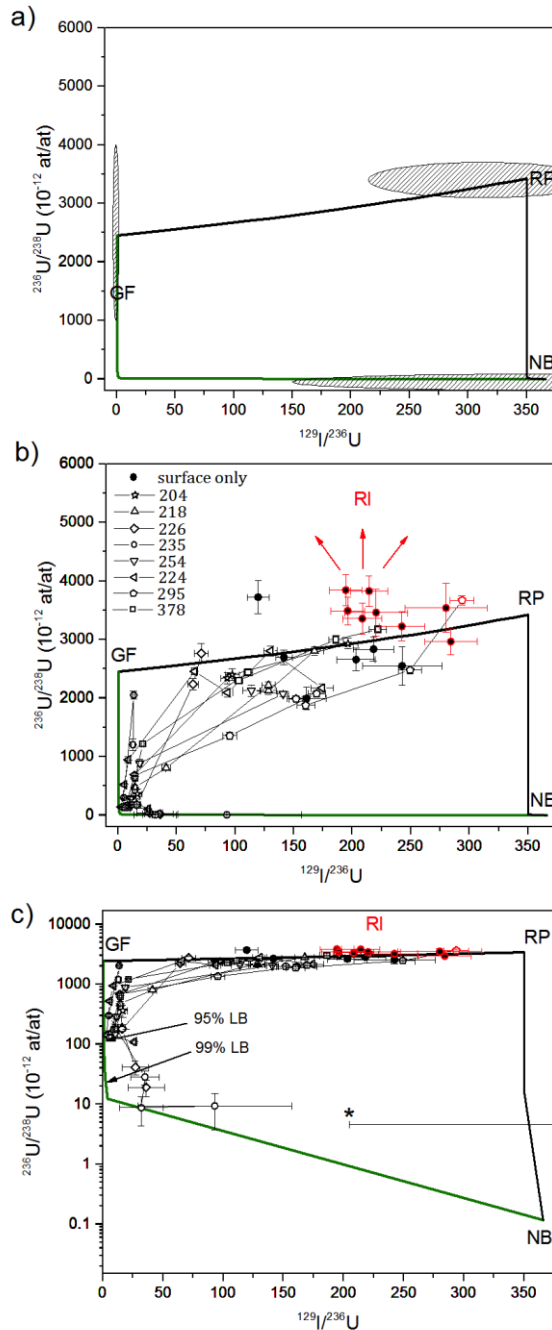
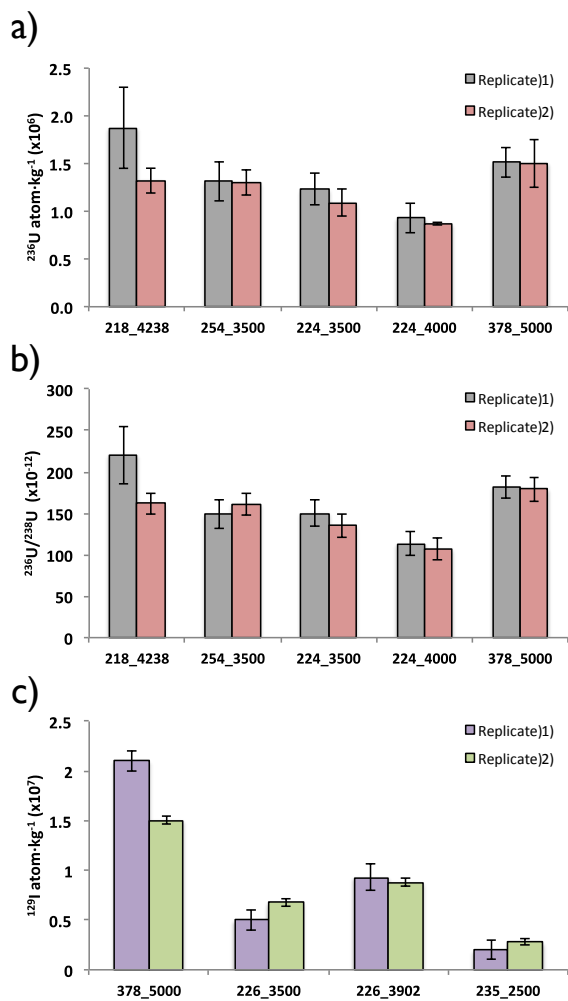


Figure 4: a) Binary mixing lines between the 3 potential sources of  $^{236}\text{U}$  and  $^{129}\text{I}$ . The domain within the mixing lines represents the different combinations of  $^{236}\text{U}$  and  $^{129}\text{I}$

concentrations depending on the contribution of the each end member (global fallout (GF), reprocessing plants (RP), and natural background (NB)). River (RI) as a potential source is represented over the GF-RP binary line. Shaded oval shape describes the range of temporal and spatial variability of each endmember (see Table 2 for details). Samples including a considerable fraction of river water are represented in red-edge color. b)  $^{129}\text{I}/^{236}\text{U}$  and  $^{236}\text{U}/^{238}\text{U}$  ratios obtained in our samples plotted on top of the mixing model. c) Same as b) but x-axis in log-scale. (\*) Is a minimum estimate, calculated from 1 sigma error of the lowest  $^{129}\text{I}$  and the highest  $^{236}\text{U}$  concentrations.



587 *Supplementary Figure: Results of the  $^{236}\text{U}$  concentrations (a),  $^{236}\text{U}/^{238}\text{U}$  atomic ratio*  
 588 *(b) and  $^{129}\text{I}$  concentrations (c) of the replicates in Table 1.*



589  
590

Supplementary table (S1): Concentrations of  $^{236}\text{U}$ ,  $^{129}\text{I}$  and  $^{236}\text{U}/^{238}\text{U}$  and  $^{129}\text{I}/^{236}\text{U}$  atomic ratios in surface samples and water column profiles in the Arctic Ocean during the ARK XXVI/3 (2011) and ARK XXVII/3 (2012) expeditions and from the Lena River mouth (2014). Acronyms for the water masses are Polar Mixed Layer (PML) and Atlantic Waters layer (AW) and were assigned according to the description by Rudels et al (2009). (1) This sample corresponds to 1 L volume water instead of 10 L. (2) Reported as a low limit, which is calculated from 1 sigma error of the lowest  $^{129}\text{I}$  and the highest  $^{236}\text{U}$  concentrations. (3) Replicate was done for  $^{236}\text{U}$ . (4) Replicate was done for  $^{129}\text{I}$ .

(This table is included as supplementary material)

23 Table 1: Results of  $^{236}\text{U}$  and  $^{129}\text{I}$  and  $^{236}\text{U}/^{238}\text{U}$  in replicated samples. Errors are at 1  $\sigma$  range.

| Station | Depth (m) | Replicate # | $^{236}\text{U}$ conc.               |       | $^{236}\text{U}/^{238}\text{U}$ atom ratio |       | $^{129}\text{I}$ conc.               |       |
|---------|-----------|-------------|--------------------------------------|-------|--|-------|--------------------------------------|-------|
|         |           |             | $10^6 \text{ at}\cdot\text{kg}^{-1}$ | $\pm$ | $10^{-12}$                                 | $\pm$ | $10^7 \text{ at}\cdot\text{kg}^{-1}$ | $\pm$ |
| 218     | 4238      | 1           | 1.9                                  | 0.4   | 220  | 35    |                                      |       |
|         |           | 2           | 1.3                                  | 0.1   | 162  | 13    |                                      |       |
| 254     | 3500      | 1           | 1.3                                  | 0.2   | 149  | 17    |                                      |       |
|         |           | 2           | 1.3                                  | 0.1   | 161  | 13    |                                      |       |
| 224     | 3500      | 1           | 1.2                                  | 0.2   | 150  | 16    |                                      |       |
|         |           | 2           | 1.1                                  | 0.1   | 135  | 14    |                                      |       |
| 224     | 4000      | 1           | 0.9                                  | 0.2   | 114  | 15    |                                      |       |
|         |           | 2           | 0.87                                 | 0.01  | 107  | 13    |                                      |       |
| 378     | 500       | 1           | 1.5                                  | 0.2   | 182  | 14    |                                      |       |
|         |           | 2           | 1.5                                  | 0.3   | 179  | 15    |                                      |       |
| 226     | 3500      | 1           |                                      |       |  |       | 2.1                                  | 0.1   |
|         |           | 2           |                                      |       |  |       | 1.5                                  | 0.04  |
| 226     | 3902      | 1           |                                      |       |  |       | 0.5                                  | 0.1   |
|         |           | 2           |                                      |       |  |       | 0.68                                 | 0.04  |
| 235     | 2500      | 1           |                                      |       |  |       | 0.9                                  | 0.1   |
|         |           | 2           |                                      |       |  |       | 0.88                                 | 0.04  |
| 235     | 3000      | 1           |                                      |       |  |       | 0.2                                  | 0.1   |
|         |           | 2           |                                      |       |  |       | 0.28                                 | 0.03  |

24

25

26

27 Table 2: Concentrations of  $^{129}\text{I}$ ,  $^{236}\text{U}$  and  $^{129}\text{I}/^{236}\text{U}$ ,  $^{236}\text{U}/^{238}\text{U}$  atomic ratios defined for the three endmembers: Natural Background (NB), Global  
 28 Fallout (GF) and Reprocessing Plants (RP). Concentration of  $^{238}\text{U}$  is considered to be constant in all endmembers, of 3.3 ppb ( $8.35 \times 10^{15} \text{ at}\cdot\text{l}^{-1}$ ) as  
 29 any other contribution of  $^{238}\text{U}$  from other sources would immediately be negligible compared to the seawater concentration.

| Endmember                | $^{129}\text{I}$<br>( $\text{at}\cdot\text{l}^{-1}$ )                                      | $^{236}\text{U}$<br>( $\text{at}\cdot\text{l}^{-1}$ ) | $^{129}\text{I}/^{236}\text{U}$                 | $^{236}\text{U}/^{238}\text{U}$   |
|--------------------------|--|---|---|---|
| Natural Background (NB)  | Average: $3.6 \times 10^5$ (1)<br>Minimum: $1.6 \times 10^5$<br>Maximum: $4.4 \times 10^5$ | $\leq 9.8 \times 10^2$ (2)                            | Average: 366<br>Minimum: 150<br>Maximum: 450    | $\leq 1.2 \times 10^{-13}$  |
| Global Fallout (GF)      | $1 \times 10^7$ (3)  | $2.05 \times 10^7$                                    | 0.5   | Average: $2.5 \times 10^{-9}$ (4)<br>Minimum: $1 \times 10^{-9}$<br>Maximum: $4 \times 10^{-9}$ (5) |
| Reprocessing Plants (RP) | $1 \times 10^{10}$ (6)   | $2.9 \times 10^7$                                     | Average: 350 (7)<br>Minimum: 215<br>Maximum 410 | $3.42 \times 10^{-9}$ ( $\pm 15\%$ )  |

(1) Considering 100 kg of  $^{129}\text{I}$  in oceans (Raisbeck and Yiou., 1999), and references.

(2) Considering 0.5 kg of  $^{236}\text{U}$  in oceans (Steier et al., 2008)

(3) From He et al. (2011)

(4) Average value from Winkler et al (2012).

(5) Maximum concentrations in Winkler et al (2012) recalculated to latitudinal belt 30-60°, Northern Hemisphere, where maximum fallout was deposited.

(6) Estimated from Christl et al. (2015)

(7) Estimated from the sum of the releases of  $^{129}\text{I}$  and  $^{236}\text{U}$  of Sellafield and La Hague in the last 10 years.